DEVELOPMENTAL BIOLOGY

Convergent deployment of ancestral functions during the evolution of mammalian flight membranes

Charles Y. Feigin[1,2], Jorge A. Moreno[1], Raul Ramos[3], Sarah A. Mereby[1], Ares Alivisatos[1], Wei Wang[4], Renée van Amerongen[5], Jasmin Camacho[6], John J. Rasweiler IV[7], Richard R. Behringer[8], Bruce Ostrow[9], Maksim V. Plikus[3], Ricardo Mallarino[1]*

Lateral flight membranes, or patagia, have evolved repeatedly in diverse mammalian lineages. While little is known about patagium development, its recurrent evolution may suggest a shared molecular basis. By combining transcriptomics, developmental experiments, and mouse transgenics, we demonstrate that lateral *Wnt5a* expression in the marsupial sugar glider (*Petaurus breviceps*) promotes the differentiation of its patagium primordium. We further show that this function of *Wnt5a* reprises ancestral roles in skin morphogenesis predating mammalian flight and has been convergently used during patagium evolution in eutherian bats. Moreover, we find that many genes involved in limb development have been redeployed during patagium outgrowth in both the sugar glider and bat. Together, our findings reveal that deeply conserved genetic toolkits contribute to the evolutionary transition to flight in mammals.

INTRODUCTION

Flight has arisen as many as seven times among extant mammals. This includes bats, which evolved powered flight, as well as six instances of unpowered flight, or gliding, in diverse taxa such as colugos, flying squirrels, and marsupial possums (*1*–*4*). Each flying lineage has evolved a lateral flight membrane, or patagium, between the fore- and hindlimbs. This structure acts as an airfoil, generating lift and permitting directional movement during flight (Fig. 1A) (*5*). Notably, a lateral patagium has arisen independently across a wide range of evolutionary divergences, from ~30 million years among some possums to the massive gulf of ~160 million years that separate marsupial and eutherian mammals (*2*, *6*, *7*). Presently, little is known about the regulation of lateral patagium development in these species. However, the repeated evolution of this structure among diverse mammals suggests that it may be derived from shared ancestral developmental programs, whose barriers to evolutionary redeployment in the skin may be small and easily overcome. Therefore, resolving the molecular basis of patagium formation may yield generalizable findings about mammalian development and insights into how phenotypic novelty emerges from evolutionarily conserved programs.

To uncover the mechanisms governing lateral patagium formation, we have developed genomic and experimental resources in an emerging model species, the marsupial sugar glider (*Petaurus breviceps*). Similar to other marsupials, sugar gliders give birth to extremely altricial young that are developmentally comparable to the fetuses of eutherian mammals (*8*, *9*). These neonates complete much of their development ex utero inside their mother's pouch and are thus referred to as pouch young (Fig. 1A) (*8*). Notably, the patagium is not discernable externally at birth in sugar glider pouch young (Fig. 1B). Rather, outgrowth of this structure begins several days postpartum. Together, the experimental accessibility of the skin, the postnatal formation of the patagium, and the sugar glider's amenability to captive husbandry make this a tractable model system to uncover how spatially patterned morphological structures originate.

RESULTS

Characterization of lateral patagium formation in the sugar glider

We first characterized lateral patagium development in the sugar glider during the first 2 weeks postpartum. We observed that pouch young first show external evidence of the patagium at approximately 5 days after birth [postnatal day 4 (P4)], in the form of a lateral ridge, most visible at the axilla. This ridge then extends outward over several weeks, gradually filling the interlimb space (Fig. 1B). Next, we examined the development of the patagium histologically, comparing it to neighboring skin along the dorso-ventral axis in transverse sections (Fig. 1, C to F). At P1, before the initiation of outgrowth, we observed an uneven distribution of nuclei in the dermal mesenchyme [indicated by 4′,6-diamidino-2-phenylindole (DAPI) staining], with higher cell density in the interlimb lateral skin that constitutes the patagium primordium, relative to more dorsal and ventral skin regions (Fig. 1, C and F). This disparity was subsequently maintained during patagium outgrowth. Of particular note, we observed a central condensate of dermal mesenchyme marking the position of the nascent patagium primordium (Fig. 1C). This condensate was just discernable at P1 but became more prominent before the initiation of patagium outgrowth. We also observed substantial thickening (hyperplasia) in the epidermis overlying this mesenchymal condensate, a phenotype that declined with greater dorsal and ventral distance from the

[1]Department of Molecular Biology, Princeton University, Princeton, NJ 08544, USA. [2]School of BioSciences, The University of Melbourne, Parkville, Victoria 3010, Australia. [3]Department of Developmental and Cell Biology, University of California Irvine, Irvine, CA 92697, USA. [4]Lewis Sigler Institute, Princeton University, Princeton, NJ 08544, USA. [5]Swammerdam Institute for Life Sciences, University of Amsterdam, Amsterdam, Netherlands. [6]Stowers Institute for Medical Research, Kansas City, MO 64110, USA. [7]Department of Obstetrics and Gynecology, State University of New York Downstate Medical Center, Brooklyn, NY 11203, USA. [8]Department of Genetics, University of Texas MD Anderson Cancer Center, Houston, TX 77030, USA. [9]Department of Biology, Grand Valley State University, Allendale, MI 49401, USA.
*Corresponding author. Email: rmallarino@princeton.edu

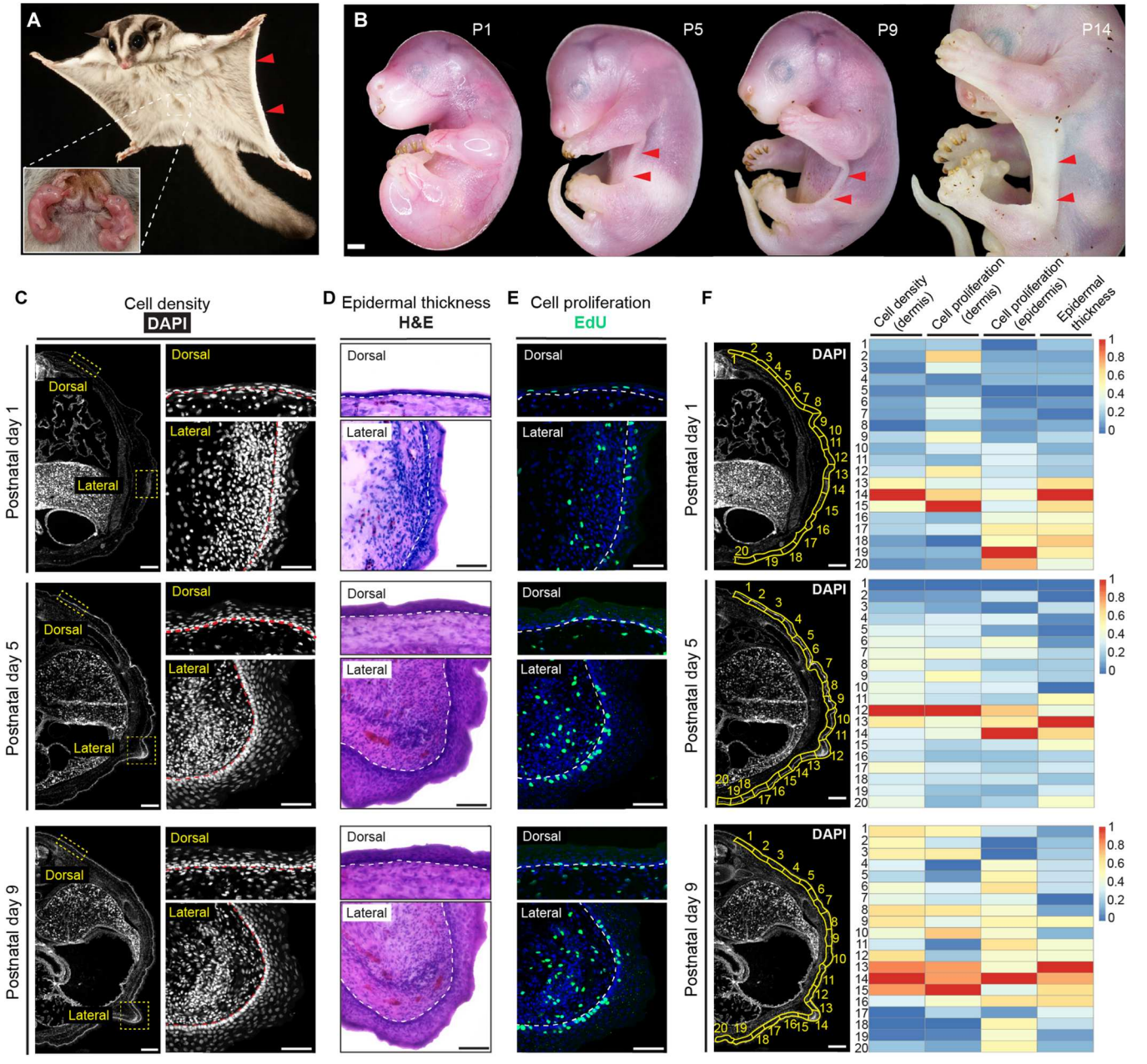

Fig. 1. Development of the lateral patagium in the sugar glider. (**A**) An adult sugar glider in flight. Red arrows indicate the lateral patagium. Inset image shows pouch young laying atop the everted maternal pouch. (**B**) Development of sugar glider pouch young during the first 2 weeks postpartum. Red arrowheads indicate position of the lateral patagium. (**C**) DAPI (4′,6-diamidino-2-phenylindole)–stained transverse sections illustrating elevated cell density in the patagium primordium relative to dorsal skin. (**D**) Hematoxylin and eosin (H&E)–stained transverse sections showing elevated epidermal thickness in the patagium primordium relative to dorsal skin. (**E**) Transverse sections showing elevated cell proliferation in the patagium primordium relative to dorsal skin, as indicated by higher EdU incorporation. (**F**) Quantification of the histological properties of sugar glider skin along the dorsal-ventral axis in transverse sections. Cell density of the dermis, thickness of the epidermis, and cell proliferation of both tissue layers were quantified within the illustrated regions of interest (ROIs), outlined in yellow, and presented as a heatmap. Dotted lines in (C) to (E) delineate the dermis-epidermis boundary. Scale bars, 1 mm (B), 500 μm (zoomed out) and 100 μm (zoomed in) (C), 100 μm (D), 100 μm (E), and 500 μm (F). Photo credit: (A) Joe McDonald, McDonald Wildlife Photography.

patagium primordium (Fig. 1, D and F). Intraperitoneal injections of pouch young with the proliferation marker 5-ethynyl-2′-deoxyuridine (EdU) revealed elevated cell proliferation in the dermal layer of the patagium primordium relative to neighboring skin (Fig. 1, E and F, and movie S1). This increase was especially pronounced in the mesenchymal condensate and in the epidermal basal layer immediately above it as development progressed, suggesting that proliferation may contribute to the establishment of observed morphological phenotypes in the dermal and epidermal layers. Together, these observations indicate that patagium formation is composed of an initial phase of histological differentiation of the primordium, marked by increased cell proliferation, dermal condensation, and epidermal hyperplasia in the patagium primordium, followed by a subsequent outgrowth phase that ultimately produces the flight membrane. Given this, we next sought to investigate the molecular basis of these developmental processes.

The sugar glider genome

To facilitate functional genomic interrogations of patagium formation, we generated a draft genome assembly for the sugar glider using approximately 240 gigabases of linked reads (10X Genomics) (*10*). The resulting assembly was ~3.4 gigabases in length, had a scaffold N50 of ~28 megabases, and was highly contiguous, with less than 2% gaps (table S1). The recovery of complete, single-copy mammalian BUSCOs (Benchmarking Universal Single-Copy Orthologs) was 86.5% comparable to other recently released genomes of related diprotodont marsupials (fig. S1 and table S2). We next annotated sugar glider genes by integrating multiple lines of transcript and protein alignment evidence, as well as ab initio gene predictions (*11*–*13*). This yielded 26,489 gene models, the identities of which were inferred by conditional reciprocal best blast searches against koala (*Phascolarctos cinereus*) RefSeq transcripts (*12*, *14*). Our sugar glider draft assembly represents a valuable resource for functional and evolutionary genomic studies.

Localized elevation of Wnt signaling in the patagium primordium

Given that patagium outgrowth is anticipated by localized histological changes in the lateral skin, we next sought to identify potential molecular drivers of this differentiation. To accomplish this, we performed RNA sequencing (RNA-seq) on patagium skin samples from sugar glider pouch young spanning the first 3 weeks of postnatal development ($n = 34$; table S3) and used weighted gene correlation network analysis (WGCNA) to predict modules of genes with highly correlated expression levels across samples (*15*). These correlation modules can reflect functional interactions between their constituent genes or roles in concurrent biological processes. WGCNA analysis predicted 13 correlation network modules, each showing distinct patterns of module eigengene expression (a summary metric for the relative expression levels of its constituent genes) over the course of patagium development (Fig. 2A). Of particular interest was patagium module 8 (hereafter PM8), a relatively small module containing only ~4.32% of patagium-expressed genes (Fig. 2A and table S4). PM8 exhibited a stronger inverse correlation ($r = -0.77$, $P < 0.001$) between its eigengene expression and animal weight (a proxy for age) than did other modules. Thus, the period of highest expression for its constituent genes corresponded closely with the onset of histological differentiation in the patagium primordium. Notably, Gene Ontology analysis indicated that PM8 was highly enriched for Wnt signaling genes (tables S5 and S6) (*16*). The results of our WGCNA analysis suggested that, while genes with roles in later patagium development may be distributed across many modules (potentially reflecting an increasingly complex tissue composition as the structure matures), PM8 genes may play a key role in morphological differentiation of the patagium primordium before its subsequent outgrowth. Moreover, Wnt signaling, particularly, may be an important regulator of this process.

If localized changes in Wnt signaling contribute to the early differentiation of the patagium as our data suggest, then we should expect this to be reflected by differences in gene expression levels relative to neighboring, non-patagium skin. Therefore, we compared the transcriptome of the skin constituting the patagium primordium to that of stage-matched samples of neighboring dorsal skin, before the initiation of patagium outgrowth ($n = 6$). Differential gene expression analysis showed that, indeed, the expression levels of many of the Wnt signaling genes belonging to PM8 were significantly greater in the patagium primordium relative to the dorsal skin (Fig. 2B and table S7) (*17*). Up-regulated genes included those encoding the Wnt family ligands *Wnt5a* and *Wnt11* as well as the Wnt signaling modulator *Dkk2*. These three secreted factors are generally associated with the activation of noncanonical Wnt signaling and/or suppression of canonical Wnt/β-catenin signaling (*18*–*20*). While this observation is consistent with a distinct Wnt signaling environment during the differentiation of the patagium primordium, these results may alternatively be explained by more general characteristics of lateral skin, rather than of the patagium specifically. To explore this possibility, we sequenced RNA from stage-matched samples of shoulder skin ($n = 6$), which sits on the opposite side of the forelimb from the patagium and occupies the same coronal plane, thus constituting a non-patagium lateral skin region (table S8). As with our comparisons against dorsal skin, roughly the same complement of PM8 Wnt signaling genes was found to be up-regulated in the patagium primordium relative to shoulder skin. Several of these genes (e.g., *Wnt5a*, *Dkk2*, *Sulf1*, and *Sulf2*) showed even larger fold increases (Fig. 2C). This analysis further supports localized elevation of Wnt signaling being a distinct molecular feature of the interlimb lateral skin comprising the patagium primordium.

Wnt signaling primarily regulates morphogenesis through intercellular communication, mediated by diffusible factors (*21*). Given this, we next characterized the spatial distribution of cells expressing the most strongly up-regulated PM8 Wnt signaling factors, *Wnt5a*, *Wnt11*, and *Dkk2*. Fluorescence in situ hybridization (FISH) showed that expression of these genes was strong in the mesenchymal condensate of the patagium primordium and extended into the overlying basal layer of the thickened epidermis above (Fig. 2D). By contrast, few cells expressed these genes in the dorsal skin. The spatial and temporal expression pattern of Wnt signaling genes further indicated that this pathway could play roles in driving differentiation of the patagium primordium. Therefore, we next sought to test for such roles through functional studies.

WNT5A drives epidermal hyperplasia in the sugar glider′s patagium primordium

The Wnt-expressing mesenchymal condensate of the patagium primordium is overlaid by a region of epidermal hyperplasia (Fig. 1, C to F, and Fig. 2D). This spatial correspondence led us to hypothesize that the mesenchymal condensate may act as a signaling center,

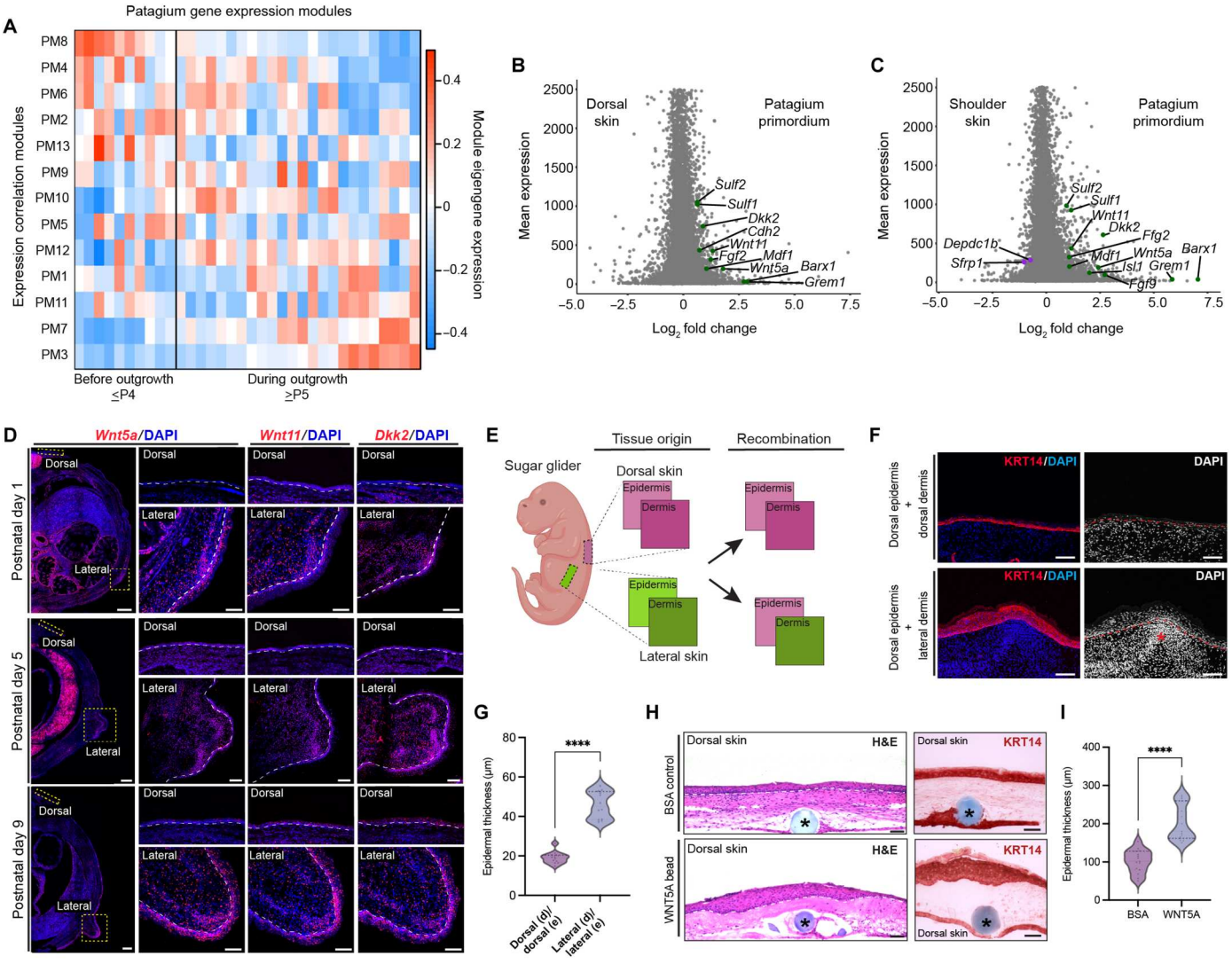

Fig. 2. A distinct transcriptomic landscape drives the establishment of early patagium phenotypes. (**A**) Heatmap displaying eigengene expression of WGCNA modules across early patagium development. Columns represent individuals, sorted by increasing weight. Rows represent modules, sorted by their correlation with sample age. Cell color represents module eigengene expression. (**B** and **C**) Genes differentially expressed between the patagium primordium and dorsal (B) or shoulder skin (C). Labeled genes are those that were both differentially expressed in the patagium primordium relative to comparison skin regions (up-regulated shown in green, and down-regulated shown in purple) and belonged to the enriched Wnt-signaling Gene Ontology term (GO:0030111). (**D**) In situ hybridizations of *Wnt5a*, *Wnt11*, and *Dkk2*. (**E**) Schematic of tissue recombination experiments. (**F**) Explants stained for KRT4 and DAPI. Asterisk denotes the mesenchymal condensate. (**G**) Quantification of epidermal thickness in recombination experiments. (**H**) H&E- and KRT14-stained, bead-implanted explants. Asterisk shows implanted bead. (**I**) Quantification of epidermal thickness in bead-implanted explants. Statistical significance in (G) (****$P < 0.0001$; $n = 5$) and (I) (****$P < 0.0001$; $n = 4$) was assessed using a general mixed effects model ANOVA test. Dotted lines in (D) and (H) delineate the dermis-epidermis boundary. Scale bars, 400 μm (zoomed out) and 100 μm (zoomed in) (D), 100 μm (F), and 200 μm (H).

controlling the thickness of the overlying epidermis. To test this, we performed epidermal-dermal tissue recombinations between the patagium and dorsal skin of sugar glider pouch young in an explant culture system. Briefly, we isolated samples of patagium and dorsal skin from pouch young just before the initiation of patagium outgrowth at P4, when the mesenchymal condensate was most prominent. We then enzymatically dissociated the two tissue layers and recombined segments of dorsal epidermis with patagium dermis ($n = 5$) or dorsal epidermis with dorsal dermis as a control ($n = 5$) and cultured them as explants for 72 hours (Fig. 2E). Immunohistochemistry (IHC) for keratin 14 (KRT14), a marker of the basal epidermal layer, showed that dorsal epidermises cultured on patagium dermises increased in thickness relative to controls (Fig. 2, F and G). This phenotype resembled differences in epidermal thickness observed between the patagium and dorsal skin in vivo (Fig. 1, C and F) and is consistent with our hypothesis that signals in the condensed mesenchyme of the patagium primordium control the thickness of the overlying epidermis.

Having demonstrated that signals from condensed dermal mesenchyme do indeed drive epidermal hyperplasia, we next asked whether this effect may be regulated by Wnt signals in particular. Among genes encoding Wnt family ligands in PM8, *Wnt5a* was

the mostly highly up-regulated in the patagium primordium compared to neighboring skin regions (Fig. 2, B and C). The *Wnt5a* ligand is a well-known morphogen that regulates the development of multiple structures during embryogenesis and plays a key role driving distal-specific gene expression (*22*). For instance, *Wnt5a* expression in dermal fibroblasts induces the expression of keratin 9 (*Krt9*), an epidermal differentiation gene expressed in acral skin regions such as the palms and soles (*23*). Moreover, dermal *Wnt5a* up-regulation has been implicated in psoriasis, a chronic skin disease characterized by pathologic epidermal hyperplasia (*24*, *25*). We therefore tested the capacity of *Wnt5a* to drive epidermal hyperplasia in sugar glider skin by soaking beads in recombinant WNT5A or bovine serum albumin (BSA) as a control and implanting them into the dermis of dorsal skin explants taken from pouch young. Consistent with our hypothesis, explants cultured with dermally implanted, WNT5A-soaked beads showed a marked increase in epidermal thickness compared to BSA-treated control explants (Fig. 2, H and I), resembling the phenotype produced by recombining dorsal epidermis with patagium dermis (Fig. 2, F and G). This finding supports a key role for locally elevated *Wnt5a* in mediating dermal control of epidermal hyperplasia in the earliest stages of patagium differentiation.

Wnt5a promotes dermal condensation in mammalian skin

Wnt5a is involved in the formation of diverse mesenchymal condensates during animal development, including chondrogenic condensates during bone development in the distal limb (*26*) and dermal condensates (precursors of the dermal papillae) during hair follicle formation (*27*). Therefore, we next asked whether *Wnt5a* may also contribute to the formation of the mesenchymal condensate observed in the patagium primordium. To this end, we leveraged the genetic tools available in the laboratory mouse (*Mus musculus*) by generating transgenic lines in which *Wnt5a* could be inducibly up-regulated (*R26rtTA;tetO-Wnt5a*) by treating animals with doxycycline (*28*, *29*). Examination of mouse skin at P37 revealed that induction of *Wnt5a* overexpression for 7 days drove a marked increase in dermal cell density in double-transgenic mice ($R26rtTA^{HET}$;$tetO\text{-}Wnt5a^{HET}$; $n = 4$) compared to doxycycline-treated control littermates ($R26rtTA^{WT}$;$tetO\text{-}Wnt5a^{HET}$; $n = 4$) (Fig. 3, A and B). Relative to *Wnt5a* expression in the patagium primordium of sugar glider pouch young, our transgenic mouse model drives relatively uniform up-regulation of *Wnt5a* throughout the skin. Thus, no discrete, lateral mesenchymal condensate was formed. Nonetheless, this finding supports *Wnt5a*'s ability to drive mesenchymal condensation in the skin of mammals, consistent with such a role in the patagium primordium. As occurred in our sugar glider explant experiments, we also observed epidermal hyperplasia in double-transgenic mice compared to controls, as evidenced by histology and IHC for KRT14, further supporting the role of *Wnt5a* in driving this phenotype (Fig. 3, C and D). Together, our experiments indicate that localized Wnt signaling, mediated in part by *Wnt5a*, coordinates the differentiation of both dermal and epidermal layers in the patagium primordium of the sugar glider.

Convergent deployment of an ancestral WNT5A function in skin morphogenesis

It is notable that induction of *Wnt5a* is able to drive phenotypes reminiscent of those observed during early patagium differentiation in the sugar glider in the skin of a mouse, a species that is fully terrestrial and last shared a common therian mammal ancestor with sugar gliders ~160 million years ago (*7*). This observation may indicate an ancestral origin for *Wnt5a*'s function in skin morphogenesis that long precedes the evolution of mammalian flight. If this is the case, then roles for *Wnt5a* in condensation of dermal mesenchyme and epidermal thickening should be discernable in the skin of other mammalian structures unrelated to flight. To examine this possibility, we next asked whether *Wnt5a* expression corresponded with patagium primordium–like phenotypes in other naturally evolved structures. To this end, we examined the skin of a distinct structure common to therian mammals and unrelated to flight: the pinna of the ear. We collected laboratory mouse samples at embryonic day 14.5 (E14.5; $n = 3$), representing an early stage in the formation of the pinna, after the initial differentiation of the epidermis (confirmed by KRT14 IHC) but before the differentiation of chondrocytes from embryonic mesenchyme (confirmed by SOX9 IHC) (Fig. 3, E and F, and fig. S2) (*30*).

Quantification of cell density by DAPI showed that, similar to the patagium in the sugar glider, the mouse pinna had a marked increase in mesenchymal density relative to neighboring head skin along the rostro-caudal axis, corresponding to tissue that will form the ear dermis and ear cartilage later in development (Fig. 3, F to H). IHC for KRT14 showed that, in addition, epidermis overlying the distal pinna exhibited hyperplasia relative to neighboring skin of the head (Fig. 3, F, G and I). Given this, we next performed fluorescent in situ hybridization to examine the spatial distribution of *Wnt5a*-expressing cells. This revealed that *Wnt5a* was robustly expressed within the mesenchyme of the pinna, with the strongest expression near the distal tip where epidermal thickness peaked (Fig. 3J). Moreover, we found that *Wnt5a* expression was nearly absent from neighboring head skin (Fig. 3J). These observations support an ancestral origin for *Wnt5a*'s function in mammalian skin morphogenesis.

Given that the role of *Wnt5a* in skin morphogenesis appears to predate the origin of flight, this role should, in principle, be part of the shared, ancestral developmental genetic toolkit of distantly related mammals. This raised the question of whether *Wnt5a* might also be involved in the early stages of patagium formation in other flying mammals that have independently evolved a lateral patagium. To explore this possibility, we acquired field-collected embryonic samples of the microbat *Carollia perspicillata* within a narrow developmental window (stages 15 to 17). This period corresponds to the early external formation of the lateral patagium, which in bats is referred to as the plagiopatagium to distinguish it from several other developmentally distinct membranes comprising the bat wing. We then performed histological analyses and compared their results to those in the sugar glider (Fig. 4, A and B) (*31*).

Transverse sections from the developing bat plagiopatagium revealed notable similarities with the patagium of the sugar glider. Relative to neighboring skin along the dorso-ventral axis, the bat plagiopatagium showed a marked increase in mesenchymal cell density (Fig. 4, C and D). Moreover, we observed a corresponding thickening of the overlying epidermis (Fig. 4, C and D). These phenotypes strongly resembled those driven by *Wnt5a* in sugar glider explants and in *Wnt5a*-overexpressing mice. Notably, although we observed that, in contrast to the sugar glider, no central mesenchymal condensate was discernable. Rather, a broader area of mesenchyme within the nascent plagiopatagium was found to be

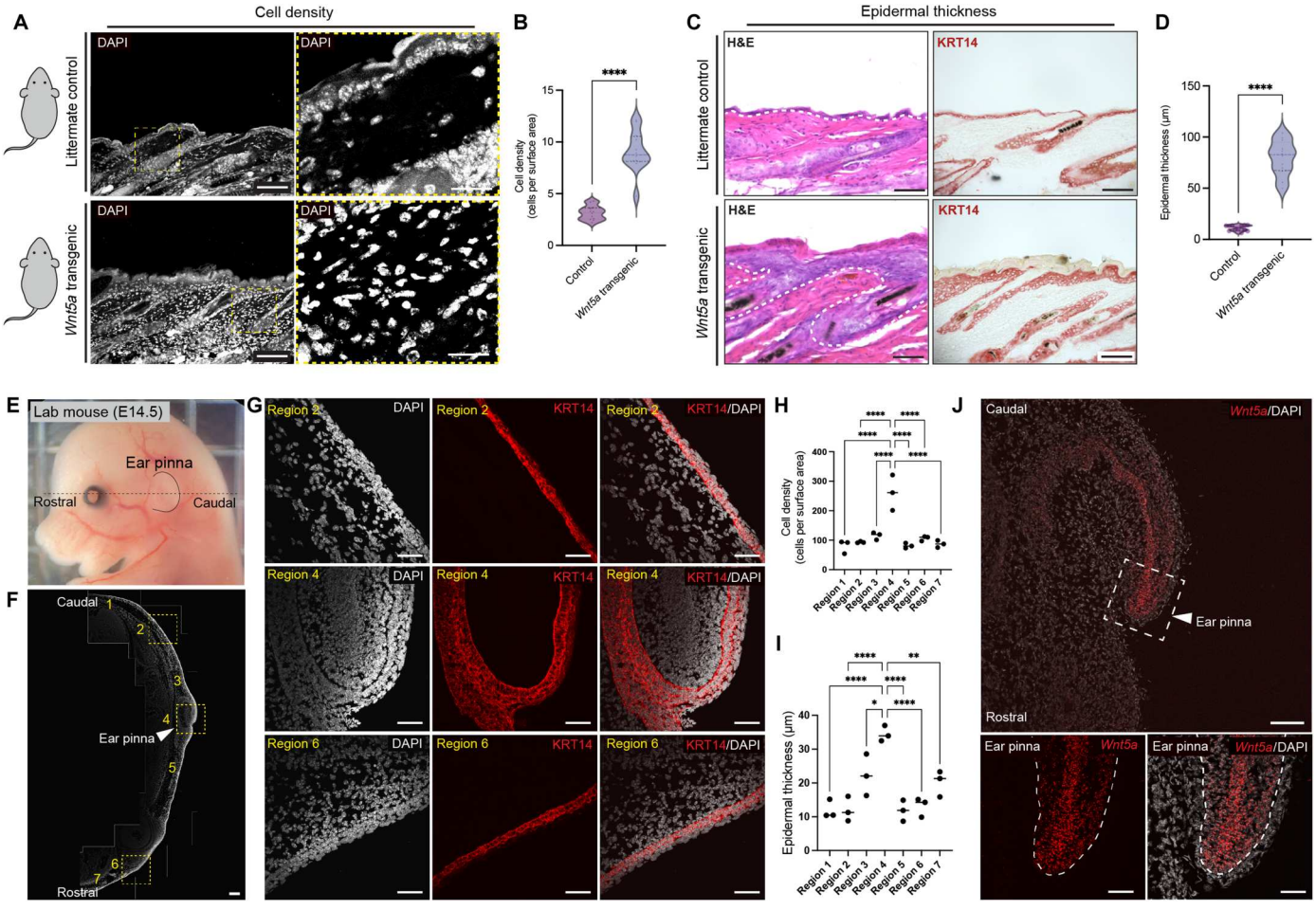

Fig. 3. *Wnt5a*'s role in skin morphogenesis is ancestral in mammals. (**A**) DAPI-stained transverse sections showing dermal cell density in transgenic mice and controls. Yellow box denotes zoomed-in region. (**B**) Quantification of cell density in transgenic mice and controls. (**C**) H&E and KRT14 stained mouse skin from transgenic mice and controls. (**D**) Quantification of epidermal thickness in transgenic mice and controls. (**E**) E14.5 mouse showing the early ear pinna. Dotted line shows the rostro-caudal axis along which sections were taken. (**F**) ROIs used for quantifying dermal cell density and epidermal thickness. (**G**) Sections stained with DAPI and KRT14. (**H** and **I**) Quantification of cell density (H) and epidermal thickness (I) in E14.5 mouse pinna. (**J**) In situ hybridization for *Wnt5a* in E14.5 mouse pinna. Statistical significance in (B) and (D) ($n = 4$; ****$P < 0.001$) and in (H) and (I) (****$P < 0.0001$, **$P < 0.01$, and *$P < 0.05$; $n = 3$) was assessed using a general mixed effects model ANOVA test. Post hoc pairwise comparisons indicated that region 4 was significantly different from other regions. All other comparisons were statistically not significant and are not displayed. Dotted lines in (C) and (J) delineate the dermis-epidermis boundary. Scale bars, 200 μm (zoomed out) and 50 μm (zoomed in) (A), 100 μm (C), 200 μm (F), 50 μm (G), and 100 μm (zoomed out) and 50 μm (zoomed in) (J).

compacted relative to neighboring skin. IHC revealed that this broader region of condensation corresponded with a similarly broad expression pattern of WNT5A within the developing plagiopatagium and an extension of its expression into the overlying epidermis (Fig. 4, E and F). As indicated by our *Wnt5a*-overexpressing transgenic mice (Fig. 3, A to D), a broader expression domain of WNT5A in the bat plagiopatagium may help explain why this structure exhibits a broader region of mesenchymal condensation (Fig. 4F) rather than a single, discrete mesenchymal condensate comparable to that seen in the sugar glider (Fig. 2D). The reliance on field-collected bat embryos, unfortunately, limits our ability to directly test for identical functional roles for WNT5A in eutherian bats akin to those observed in marsupial sugar gliders or *Wnt5a*–up-regulating transgenic mice through in vivo or explant experiments.

Together, our findings demonstrate a key role for altered expression of Wnt signaling genes, particularly *Wnt5a*, in driving early differentiation of the lateral patagium in the sugar glider. Moreover, we find evidence that this function is ancestral to mammals and has been convergently used during the evolution of flight in the eutherian bats despite their large evolutionary separation from marsupials.

Convergent deployment of limb development genes in the lateral patagia

Specification of the lateral patagium to the same coronal plane as the limbs is a functional necessity in both sugar gliders and bats, as a physical connection between these two morphological structures is ultimately required to regulate tension of the aerodynamic surface and to control direction during flight (*32*). In addition to a limb-like lateral position, it is notable that the lateral patagium's

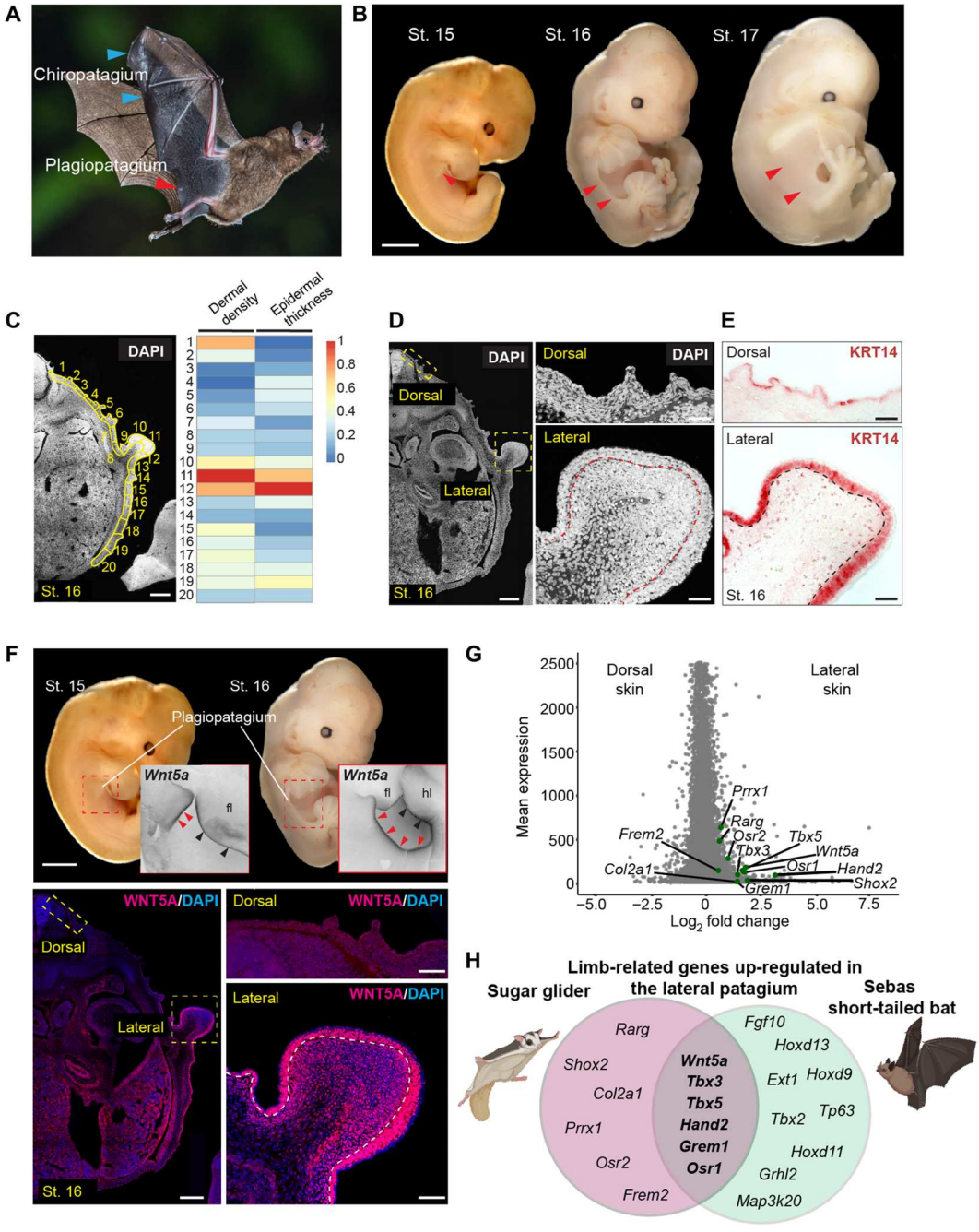

Fig. 4. Evolutionary convergence between the lateral patagia of sugar gliders and bats. (**A**) Plagiopatagium (red arrowheads) of Seba's short-tailed bat is shown in an adult animal and (**B**) in embryonic stages. This structure differs from other patagia in the bat wing, such as the chiropatagium (blue arrowheads). (**C**) Quantification of dermal cell density and epidermal thickness along the dorsal-ventral axis in an embryonic bat (St. 16) within multiple ROIs (highlighted in yellow) and illustrated in a heatmap. (**D** and **E**) Bat plagiopatagium relative to dorsal skin in transverse sections, with cell density visualized by DAPI (D) and epidermal thickness visualized by IHC for KRT14 (E). (**F**) *Wnt5a* whole-mount in situ hybridization (top images) and WNT5A IHC in transverse sections (bottom images) of embryonic bat tissue showing the spatial distribution of this gene in the developing plagiopatagium (red arrowheads) relative to dorsal skin. *Wnt5a* is also detected in the limbs (black arrowheads) (fl, forelimbs; hl, hindlimbs). (**G**) Volcano plot of genes differentially expressed between the sugar glider patagium and the neighboring dorsal skin during its outgrowth. Patagium–up-regulated genes belonging to limb development Gene Ontology terms are labeled in green. (**H**) Venn diagram showing genes with known roles in limb outgrowth and patterning convergently up-regulated in the developing lateral patagia of sugar gliders and bats. Photo credit: (A) Andrew Morffew.

outgrowth also proceeds in a manner reminiscent to that of the limbs in both species. The patagium first becomes visible externally as lateral ridge, which then extends outward (Fig. 1B). This ridge may represent a bud, akin to that of the early limbs, albeit a highly elongated one (*33*). This pattern of bud outgrowth contrasts markedly with many other skin membranes involved in tetrapod locomotion, such as the webbing found between the toes of water birds and turtle as well as the chiropatagia of bat wings. These interdigital membranes arise largely through localized suppression of apoptosis in the early limb bud, rather than as a distinct, outgrowth of skin (*34*–*36*).

The apparent developmental analogies between the lateral patagium and limbs in terms of their shared coronal plane and bud-like outgrowth suggest a potentially deeper molecular and evolutionary relationship between these structures. *Wnt5a*, which contributes to the early differentiation of the patagium in both sugar gliders and bats, is also a known driver of tetrapod limb formation (*22*). To explore this possibility, we next tested for up-regulation of limb morphogenesis genes in the lateral patagia of sugar gliders and bats during their outgrowth phase, relative to stage-matched samples of neighboring dorsal skin (tables S3, S9, and S10). Consistent with a developmental-genetic relationship with the limbs, we observed significant enrichment of multiple limb development Gene Ontology terms among genes up-regulated in the patagia of both species, including numerous transcription factors and morphogens (Fig. 4G, fig. S3, and tables S9 to S14). Most strikingly, however, we observed a complement of genes up-regulated in both species: *Wnt5a*, the bone morphogenetic protein antagonist *Grem1*, and the transcription factors *Tbx5*, *Tbx3*, *Hand2*, and *Osr1* (Fig. 4H and table S15). *Tbx5* is necessary for the initiation of forelimb outgrowth, while *Tbx3* helps to define limb bud width and participates in a transcriptional network with *Hand2* to regulate anterior-posterior patterning (*37*–*39*). *Grem1* encodes a *Bmp*/*Tgf*β inhibitor, which similarly participates in anterior-posterior digit patterning (*40*). *Osr1*, by contrast, identifies interstitial muscle connective tissues in the limb and is known to interact with *Tbx5* in other developmental contexts (*41*, *42*).

Convergent activation of limb development genes in the sugar glider and bat reinforces the notion that spatial patterning and morphogenesis of the patagium may involve, at least partial, evolutionary redeployment of processes also involved in limb formation. Although this transcriptional convergence is limited, with more uniquely redeployed limb development genes in each species than those that are shared between them (Fig. 4H). Moreover, our transcriptomic analyses do not support wholesale recycling of key early limb programs. For instance, fibroblast growth factor (FGF) family ligands involved in signaling between the apical ectodermal ridge (AER) and mesenchyme of the developing limb during outgrowth are either not expressed in the lateral patagia of sugar gliders and bats or do not show significant differences in expression relative to neighboring dorsal skin (table S16) (*43*). Similarly, *Shh*, which is expressed in the limb bud′s zone of polarizing activity was not detected in either species′ patagium. Nonetheless, given that the limbs are ancestral to all tetrapods, redeployment of specific limb morphogenesis genes may present a parsimonious explanation for the recurrent evolution of the patagium across distantly related mammalian lineages. In-depth comparative studies on the molecular regulation of lateral patagia and limbs therefore represent a potentially valuable future direction.

DISCUSSION

Flight has evolved many times among animals. Across lineages, the core structures that permit this form of locomotion vary widely. In birds, wings evolved through modifications to the ancestral tetrapod forelimb, including changes in digit number and morphology as well as the derivation of specialized skin appendages (i.e., flight feathers). In insects, recent evidence has suggested that wings are derived from ancestral leg segments and are homologous to the tergal plate found in crustaceans (*44*). In these lineages, dedicated flight structures are thought to have evolved only once. By contrast, specialized flight structures appear to have arisen at least seven times independently among extant mammals, at a wide range of evolutionary divergences. Notably, a universal feature of both powered and unpowered flight in mammals is the growth of a membranous lateral patagium connecting the limbs. The recurrent evolution of lateral patagia in diverse mammalian lineages suggests that it may reflect shared developmental programs that predate flight.

Here, we show that the formation of the patagium primordium in the marsupial sugar glider is marked by up-regulation of Wnt signaling genes. We demonstrate that *Wnt5a*, particularly, contributes to both the condensation of dermal mesenchyme and thickening of the overlying epidermis in this region. Our studies in eutherian laboratory mice further show that this role for *Wnt5a* is likely conserved in mammals, controlling skin morphogenesis in very distinct structures, such as the pinna of the ear. Furthermore, we find evidence that this ancestral function for *Wnt5a* in skin development has been convergently used during the evolution of the lateral plagiopatagium in bats, driving similar phenotypes in both dermal and epidermal skin layers despite their ~160–million year separation (*7*).

While enhanced signaling through the *Wnt5a* ligand appears to play a role in driving early phenotypes shared between the bat and sugar glider, it is less clear what developmental requirement there might be for epidermal thickening or dermal condensation during patagium formation. It is perhaps most plausible that *Wnt5a* functions chiefly within the dermis, reprising its role in condensate formation and directional outgrowth of structures such as the limbs and phallus (*22*). In this case, epidermal hyperplasia may only be an incidental readout of a distinct mesenchymal signaling environment and might thus be interpreted as an evolutionary spandrel. Changes in the relative mechanical properties of the dermal and epidermal layers of the patagium primordium driven by *Wnt5a* may, however, also play a distinct role in promoting formation of the initial patagium ridge, for instance, through buckling morphogenesis (*45*). This process can occur when two adherent tissue layers expand at different rates, leading to mechanical instability that forces the formation of a curvature. For instance, it has been proposed that gyrification in the brain may be caused by frustration of gray matter expansion due to its physical connection to underlying, slow-growing white matter (*46*). Similar tissue buckling has also been shown in the frilled dragon (*Chlamydosaurus kingii*). This species has several highly stereotyped convex folds on the skin constituting its eponymous neck frill, which arises during embryogenesis through frustrated growth of its anterior surface (*47*). If related mechanisms are at play in flying mammals, then *Wnt5a* may drive localized stiffening of mesenchyme in the patagium primordium, thereby constraining the expansion of overlying epidermis

and promoting a convex curvature of the lateral skin, similar to that seen in the early patagium ridge (Figs. 1C and 4C).

We find further evidence of molecular convergence between sugar gliders and bats. During the patagium outgrowth phase in both species, we find many shared differentially expressed genes, including significant enrichment of genes with roles in limb development. Because limbs are ancestral to all tetrapods, components of their underlying developmental programs may represent a molecular toolkit that diverse lineages may have drawn upon during the evolution of flight. Such a process may also be selected for, as it could promote adaptive functional integration between the patagium and limbs. In both sugar gliders and bats, the patagia must be physically connected to the limbs to function. Yet, limbs and patagia do not arise simultaneously during development. Given that spatial patterning mechanisms already exist in tetrapods to specify outgrowth programs to the lateral plane during limb formation, these mechanisms may inherently provide a means to direct patagium growth to its proper location in relation to the limbs. Exploring similarities between the regulatory apparatuses of convergently redeployed genes, such as *Wnt5a*, *Tbx5*, *Tbx3*, *Hand2*, and *Osr1* in the limbs and lateral patagia, presents a valuable future direction, as it has the potential to recalibrate our understanding of the role of pleiotropy in adaptive evolution. Most often, pleiotropy is viewed as an important source of evolutionary constraint because recycling of developmental programs exposes them to greater negative selection (*48*). In the case of the patagium, however, reuse of mechanisms for spatially patterning the expression of limb outgrowth genes in a single coronal plane could hypothetically provide a means of facilitating beneficial functional integration between an ancestral structure and a novel one.

Along these lines, further study will be needed to define the mechanisms controlling localizing gene expression during patagium formation. Given the central role that cis-regulatory regions play in spatially patterned gene expression, it is plausible that these elements may contain many of the causative mutations responsible for directing genes to the lateral skin. However, the preponderance of genes differentially expressed in the patagia of sugar gliders and bats may indicate (on the basis of parsimony) that these genomic changes are focused around a smaller number of regulatory factors, which, in turn, drive much larger batteries of patagium gene expression. *Wnt5a* represents a strong candidate for such a factor given its sufficiency to drive patagium primordium phenotypes in the skin, but we cannot preclude at present that its expression is, in turn, controlled by regulatory genes further upstream.

Unpowered flight has arisen independently many times among nonmammalian vertebrates. While the lateral patagia of lizards in the genus *Draco* are composed of elongated ribs, those of the flying geckos are potentially more similar in structure to gliding mammals. Thus, our findings in the sugar glider and bat may reflect even more ancient developmental programs and thus have implications for the evolution of flight across vertebrates more broadly. Continued exploration of the gene networks governing patagium formation, particularly in a comparative context, may therefore have the potential to provide profound insights into development and adaptation.

MATERIALS AND METHODS

Sugar glider husbandry

Captive-born, adult sugar gliders were obtained from the U.S. pet trade and thereafter were maintained in breeding colonies at Princeton University and Grand Valley State University. All experiments performed were approved by the respective Institutional Animal Care and Use Committee at Princeton University and Grand Valley State University. The colonies were maintained on a 12-hour light:12-hour dark cycle, within temperature and humidity rates of 20° to 27°C and 30 to 70%, respectively. Animals were housed as bonded male-female pairs or groups of one male and two to three females and fed a diet consisting of dried food, fruits, and protein. Animals were checked for pouch young typically two to five times per week by gentle palpation of the maternal pouch and provided a drop of honey as a reward, delivered on a disposable tongue depressor. Pouch young found by palpation were visually examined by briefly anesthetizing the mother with isoflurane and gently everting the material pouch to expose the neonate. All pouch young were either found alone or as twins, with one on each side of the pouch. Pouch young, which remain attached to the nipple during the first several weeks of life, were removed while the mother was under anesthesia by gently placing the pointer finger and thumb in front of its snout and applying light pressure.

Species nomenclature

The marsupial gliders kept in the U.S. pet trade are commonly referred to as sugar gliders and belong to the *P. breviceps* species complex, whose native range extends through parts of eastern mainland Australia as well as the island of New Guinea (both Papua New Guinea and West Papua, Indonesia) (*9*). Studies over the past decade indicate that genetic relationships of populations across this range are complicated (*49*–*51*). However, previous findings suggest that gliders in the U.S. pet trade, from which our sugar glider colony was derived, originated from a source population in West Papua Indonesia, near the city of Sorong, and may have sister-group relationship to Australian populations (*51*).

It was recently proposed that several Australian populations within the *P. breviceps* complex be split into three distinct species: *P. breviceps* (sugar glider), *Petaurus notatus* (Krefft's glider), and *Petaurus ariel* (savanna glider), occupying abutting ranges in eastern Australia (*50*). However, this work did not address the relationship of New Guinean populations to those in Australia, and no new nomenclature for New Guinean populations was put forward. Considering the phylogeographic relationships previously suggested (*51*), the species divisions proposed in (*50*) would likely result in paraphyly of *P. breviceps*.

Given this, we have opted to follow previous conventions for New Guinean populations and refer to gliders in our colony as *Petaurus breviceps papuanus* (*52*). In addition, we use the common name "sugar glider" to refer to our animals, as is common practice in the pet trade. We recognize, however, that the taxonomy of the *P. breviceps* complex is currently in flux and that the current nomenclature will likely be revised. Future population genomic studies of both Australian and New Guinean *Petaurus* gliders will thus be of tremendous interest to the systematics, evolution, and conservation research communities.

Sugar glider genome sequencing, assembly, and annotation

Genome sequencing and assessment

Muscle tissue (50 mg) was obtained from a euthanized adult female sugar glider, and high–molecular weight DNA was extracted using the QIAGEN MagAttract HMW Kit (NEB, 67563). The DNA was quantified using the Qubit DNA HS Kit (Thermo Fisher Scientific, Q32851), and the fragment size was assessed using Bioanalyzer 2100 and High Sensitivity chip (Agilent, 5067). Sequencing libraries were prepared using the Genome v2 Library Prep Kit and Chromium instrument (10X Genomics). Libraries were then sequenced on an Illumina HiSeq 2500 Rapid Flow Cell to produce ~241.5 gigabytes of sequence in paired-end 2 × 200–base pair (bp) format. Reads were assembled using the SuperNova2.0 pipeline (10X Genomics) (*10*). A small number of duplicate scaffolds were identified by reciprocal blast (see below) and removed. Summary statistics for the resulting assembly were generated using the stats.sh script in the BBmap package (v37.93). The representation of mammalian universal single-copy orthologs in the sugar glider and other diprotodont marsupials was assessed with BUSCO version 5.5.2 (https://busco.ezlab.org/) using the curated mammalian version 10 database (mammalia_odb10) (*53*). Values for the common wombat (*Vombatus ursinus*), koala (*P. cinereus*), tammar wallaby (*Macropus eugenii*), quokka (*Setonyx brachyurus*), and ground cuscus (*Phalanger gymnotis*) were generated previously (*54*). Values for all other species shown were calculated in the present study.

Gene annotations

Genes in the sugar glider assembly were annotated with the Maker2 pipeline using multiple lines of evidence (*11*). Homology evidence was generated through alignment of RefSeq proteins and transcripts sequences from koala (*P. cinereus*), Tasmanian devil (*Sarophilus harrisii*), gray short-tailed opossum (*Monodelphis domestica*), tammar wallaby (*Notamacropus eugenii*), human (*Homo sapiens*), and laboratory mouse (*M. musculus*) (*12*, *14*). De novo sugar glider transcripts were assembled from RNA-seq reads using Trinity v2.7.0 with default settings (*55*). Transcripts were aligned to the genome as evidence via Maker2's expressed sequence tag (EST) option. Ab initio gene predictions were performed using the human model provided by Augustus and a sugar glider model generated using SNAP (*13*, *56*). Three annotation iterations were performed in total. In the first, only the Augustus model and alignment evidence were used (sugar glider transcripts and homologous proteins/transcripts), with parameters est2genome and protein2genome set to 1. Gene models with an annotation edit distance <0.75 were then used to generate a hidden Markov model (HMM) for SNAP. In the second iteration, the initial SNAP HMM was included along with all other evidence, and est2genome and protein2genome were set to 0. A final SNAP HMM was then produced and included in a third and final iteration. Identities were assigned to gene models by reciprocal blast implemented by crb-blast (https://github.com/cboursnell/crb-blast) against RefSeq koala transcripts (*12*, *14*). Annotations for the sugar glider were deposited in a FigShare repository (https://figshare.com/s/d6c585fbae0c1f22e8df).

Phenotypic characterization of sugar glider pouch young and bat embryos

Sample processing

Sugar gliders. Sugar glider pouch young were injected intraperitoneally with EdU (50 mg/kg; Lumiprobe) and were collected 2 hours later. Samples used for section histology were then fixed in 4% paraformaldehyde (PFA) and processed through the following overnight incubations: 10% sucrose–phosphate-buffered saline (PBS), 30% sucrose-PBS, and a 50:50 mixture of 30% sucrose-PBS and optimal cutting temperature (OCT) compound. Processed samples were then embedded in OCT (Tissue-Tek, 4583), and transverse sections of 10 to 14 μm were taken using a cryostat (Leica, CM3050S). EdU incorporation was visualized by using a labeling mix containing copper sulfate pentahydrate (2 mM; Sigma-Aldrich, 209198), ascorbic acid (20 mg/ml; Sigma-Aldrich, PHR1008), and sulfo-cyanine5 azide dye (8 μM; Lumiprobe, A3330). Samples were also washed for 10 min in a solution of DAPI (1.25×10^{-3} mg/ml; Sigma-Aldrich, D9542) in PBS to fluorescently label nuclei within tissue sections.

Bats. Bat embryos (*C. perspicillata*) were wild-collected in Trinidad under permits issued by the Wildlife Section, Forestry Division, Ministry of Agriculture, Land and Marine Resources (Republic of Trinidad and Tobago). Embryos were fixed in 4% PFA in PBS for 24 hours, rinsed in PBS, and gradually dehydrated in increasing concentrations of methanol [25, 50, 75, and 100% in double distilled water (ddH_2O), 1 hour each] and stored at −80°C. Upon arrival to the laboratory, samples were either processed for section histology and IHC, as described above, or kept in methanol for whole-mount IHC.

Confocal imaging

Confocal stacks from sections of sugar glider pouch young were generated using an A1R-STED (Stimulated Emission Depletion Detector) confocal microscope (Nikon) and processed with the accompanying NIS-Elements software (Nikon). Confocal stacks were then split into single-channel stacks (488 and 647, respectively). The brightness of each stack was adjusted to maximize the signal-to-noise ratio, and then stacks were flatted into single reference images with ImageJ′s built-in ″Z Project″ function. Binary conversion was done using ImageJ′s ″Make Binary″ function with the IsoData method and a dark background. Thresholds were calculated using the entire Z projection. The resulting images had two pixel values, 0 for black and 255 for white. All images are representative of three individuals per stage.

Quantification of epidermal thickness and proliferation

The epidermis was identified by eye using the DAPI channel in ImageJ and divided into 20 equal regions of interest (ROIs) along the dorsal-ventral axis. A segmented line was drawn following the curve of the basement membrane of the epidermis from the neural tube to the ventrum. This line was used to define 20 ROIs of equal lengths along the basement membrane, extending distally to the outer edge of the epidermis. Epidermal thickness was quantified by measuring the distance from the basement membrane to the exterior margin of the epidermis at the distal edge of each ROI. Epidermal proliferation was quantified in the EdU channel using ImageJ′s ″Analyze Particles″ function to identify dividing cells in each epidermal ROI. Images are representative of three individuals per stage.

Quantification of dermal density and proliferation

The dermis underlying each epidermal ROI was defined along the same segmented line following the curve of the epidermal basement membrane described above. A straight line 100 μm in length was drawn toward the center of the tissue section from the edge of each epidermal ROI. These lines were connected by another segmented line following the curvature of the tissue, resulting in a

region of dermis underlying each of the previously defined epidermal ROIs. The dermal density was quantified in the DAPI channel using ImageJ's "Analyze" function to find the mean fluorescence intensity of the DAPI signal for each dermal ROI. This produced a measure of the average intensity of signal adjusted for the area of the ROI. The dermal proliferation was quantified in the EdU channel using ImageJ's "Analyze Particles" function to identify dividing cells in each dermal ROI. Images are representative of three individuals per stage.

Tissue clearing and light sheet microscopy for sugar glider joeys

P3 sugar glider joeys were injected with EdU, collected 2 hours later, and fixed in 4%, as described above. Visualization of cell proliferation was carried using a modified iDISCO (immunolabeling-enabled three-dimensional imaging of solvent-cleared organs) and tissue clearing protocol (*57*, *58*). Briefly, joeys were dehydrated in increasing concentrations of methanol (25, 50, 75, and 100% in ddH_2O, 1 hour each), bleached in a 5% hydrogen peroxide (H_2O_2; Sigma-Aldrich, 1086001000)/methanol solution overnight, and serially rehydrated (methanol:ddH_2O, 1 hour each). Joeys were then washed in a solution of 20% dimethyl sulfoxide (DMSO) (Thermo Fisher Scientific, D128) + 0.3 M glycine (Sigma-Aldrich, 410225) + 0.2% Triton X-100 (Sigma-Aldrich, T8787)/PBS at 37°C for 2 days and subsequently immersed in a blocking solution of 10% DMSO + 6% donkey serum (EMD Millipore, S30) + 0.2% Triton X-100/PBS at 37°C for 3 days. After this, joeys were washed twice for 1 hour per wash in a solution containing 0.2% Tween 20 (Sigma-Aldrich, P9416) + heparin (10 mg/ml; Sigma-Aldrich, H3149)/PBS. Following this, joeys were processed for EdU incorporation using the Click-iT EdU Imaging Kit (Thermo Fisher Scientific, C10086) following the manufacturer's suggestions, except that incubation times were extended to 2 days for each step. After the final wash, samples were serially dehydrated in methanol (methanol:ddH_2O, 1 hour each), treated with 2:1 dichloromethane (DCM; Sigma-Aldrich, 270997):methanol, and then incubated in 100% DCM for 2 days. Embryos were then placed in dibenzyl ether (DBE; Sigma-Aldrich, 108014) and stored at room temperature before imaging. For imaging, joeys were glued lateral side down on a custom-designed three-dimensional printer holder and imaged in DBE using a light-sheet microscope (Ultramicroscope II, LaVision Biotec) running an ImSpector Microscope controller software (version 5.1.347). Imaging of EdU^+ cells was acquired as described previously (*58*).

Spatial analysis of gene expression

Fluorescence in situ hybridization

Starting from a pool of sugar glider skin complementary DNA (cDNA), we generated digoxigenin (DIG)-labeled riboprobes by cloning fragments of *Wnt5a* (primers: 5′-GAGACGGCC TTCACTTATGC-3′ and 5′-GTCTGCACCGTCTTGAACTG-3′), *Wnt11* (primers: 5′-AACAGCTGGAAGGACTGGTG-3′ and 5′-CACCTTGGTGGCTGATAGGT-3′), and *Dkk2* (5′-CCCAGT TACCGAAAGCATATTAACC-3′ and 5′-AAAGCCAGACTC CATGTGTGTC-3′). We carried out FISH following previously described protocols (*59*). Briefly, tissue sections were post-fixed with 4% PFA in PBS, washed with PBS, placed in triethanolamine/acetic anhydride for 20 min, and incubated overnight with riboprobes at 65°C. The following morning, probes were washed with 0.2× saline sodium citrate, equilibrated with buffer, and incubated with secondary anti-DIG antibody (1:500) for 3 hours. After washing several times, the signal was developed with the Tyramide Signal Amplification System, following the protocol suggested by the manufacturer (PerkinElmer, NEL 753001KT). Tissues were visualized using an A1R-STED confocal microscope (Nikon). All images are representative of at least three individuals per stage.

Immunohistochemistry

IHC in sections of sugar glider explants, transgenic mouse skin, and bat plagiopatagium was performed using anti-KRT14 (1:1000; BioLegend, 905303), anti-WNT5A (1:100; BiossUSA, bs-1948R), anti-Ki67 (1:100; Abcam, ab15580), and anti-SOX9 (1:250; Millipore-Sigma, AB5535). Reactions were visualized with horseradish peroxidase (HRP)–streptavidin and the 3-amino-9-ethylcarbazole (AEC) Substrate Kit (Vector Laboratories, SK4200) or Alexa dye–conjugated secondary antibodies (Thermo Fisher Scientific). Control tissue was incubated with PBS instead of primary antibodies. Cell nuclei were stained with DAPI. Sections were examined using an A1R-STED confocal microscope and an NiE upright microscope (Nikon). All images are representative of at least three individuals per stage. IHC of the mouse pinna was performed using the rabbit monoclonal cytokeratin 14 (K14) antisera (SP53; Abcam, ab119695) for 8 hours at 4°C, followed by incubation with goat anti-rabbit immunoglobulin H&L Alexa Fluor 555 (Abcam, ab150078) for 1 hour at room temperature.

Whole-mount in situ hybridization

Whole-mount in situ hybridization on bat embryos was carried out following a previously established protocol with slight modifications (*60*). Briefly, embryos were rehydrated in increasing concentrations of methanol (25, 50, 75, and 100% in PBS, 20 min each) and post-fixed in a solution containing 4% PFA + 0.1% glutaraldehyde (Sigma-Aldrich, G5882). Embryos were then treated with 5% H_2O_2 for 1 hour to block endogenous peroxidase activity, washed in PBT (1× PBS + 0.1% Tween 20), and incubated for 1 hour in blocking solution [3% BSA (Sigma-Aldrich, B4287) + PBS + 0.1% Tween 20]. Following this, we incubated embryos overnight with primary antibody diluted in blocking solution. The next morning, embryos were washed in PBS for 1 hour, treated with 3% H_2O_2 for 1 hour, and washed with PBT for 1 hour Embryos were then incubated overnight with secondary biotinylated antibody (Vector Laboratories, BP-9100-50). The following day, embryos were washed and incubated with HRP-streptavidin (Vector Laboratories, SA-5704-100) for 1 hour and developed the signal with AEC (Vector Laboratories, SK4200), following the manufacturer's instructions.

RNA scope

Cells expressing *Wnt5a* were visualized in the pinnae of E14 embryonic mice from cryosectioned tissues (12-μm sections) using the RNAscope v2 (323100, Advanced Cell Diagnostics), following the manufacturer's instructions. The *M. musculus Wnt5a* probe (Advanced Cell Diagnostics, 316791) was used. For all experiments, slides were mounted using VECTASHIELD Antifade Mounting Medium and with DAPI (Vector Laboratories, H-1200-10). Fluorescent images were captured with a FLUOVIEW 3000 laser scanning microscope (Olympus) with a UPLSAPO 10×/0.45 and 40×/1.25 Silicone objectives (Olympus).

RNA sequencing and data preprocessing

Sugar gliders

We collected 34 patagium samples from glider pouch young spanning the first 3 weeks of postnatal development, as well as dorsal skin from approximately the first 12 days postnatal and shoulder skin from approximately the first 4 days postnatal. RNA was extracted from each tissue by first lysing skin tissue with the Next Advanced Bullet Blender and then isolating the total RNA with the RNeasy Fibrous Tissue Mini Kit (QIAGEN, 74704). The RNA (100 ng) was provided to the Genomics Core Facility at the Lewis-Sigler Institute (Princeton University) for quality control and library preparation following the Smart-seq2 protocol with an average insert size of 200 bp (*61*). The size distribution and RNA integrity were measured using the Agilent Bioanalyzer 2100 and RNA 6000 Pico chip. Libraries were individually barcoded, pooled, and then sequenced at the New York Genome Center on an Illumina NovaSeq in 2 × 150–bp format. After demultiplexing, reads were filtered by quality and trimmed to remove residual adapter sequences and low-quality end bases using Trimmomatic 0.38 parameters: SLIDINGWINDOW: 5:20, MINLEN: 50, and AVGQUAL: 25 (*62*). Reads were then mapped against the sugar glider genome assembly using STAR v2.7.3a (*63*).

Bats

Bat embryos (*C. perspicillata*) were wild-collected and preserved in RNAlater (Thermo Fisher Scientific). Upon return to the laboratory, dorsal ($n = 5$) and lateral skin tissues ($n = 5$) were dissected. RNA was extracted, and its quality was assessed following the same procedures outlined above. Libraries were prepared using the directional PrepX RNA-seq library preparation protocol on the automated Apollo 324TM NGS Library Prep System (Takara Bio, CA), with a cDNA insert average size of ~200 bp.

To produce genome annotations suitable for RNA-seq analyses, we performed an annotation liftover procedure implemented in the program LiftOff v1.6.3 (parameter: -d4) to transfer gene models from the closely related microbat *Artibeus jamaicensis* (GCF_014825515.1/WHU_Ajam_v2) to the DNAZoo *C. perspicillata* assembly (*64*, *65*). This yielded 23,706 gene models used for downstream analysis. Annotations for Seba's short-tailed bat were deposited in a FigShare repository (https://figshare.com/s/d6c585fbae0c1f22e8df).

Weighted gene correlation network analysis

Network analyses were performed using WGCNA (*15*). Briefly, read counts generated by featureCounts were normalized by rlog transformation (*17*). The pickSoftThreshold function was used to estimate scale-free threshold for each dataset, testing soft power thresholds from 1 to 30 in increments of 1. We chose a scale-free topology of 0.8 (80%), which was achieved at a soft power threshold of 11. An unsigned correlation network was then constructed with the blockwiseModules function using the soft power threshold determined above. Gene correlation calculations are agnostic of sample stage or weight. Therefore, after module construction samples were ordered by developmental stage and animal weight, per-sample module eigengene values of each module were plotted as a heatmap (Fig. 2A). The correlation coefficient (weighted Pearson correlation) between PM8 module eigengene expression and animal weight (a proxy for age) was calculated, and its significance was assessed by Student's *t* test using WGCNA's included cor and corPvalueStudent functions, respectively (*15*). PM8 genes were examined for Gene Ontology term enrichment via the Gene Ontology Resource Web server (http://geneontology.org/) using the *M. musculus* biological process database. The term enrichment significance was determined by Fisher's exact test [false discovery rate (FDR) < 0.05].

Differential gene expression analyses

Pairwise differential expression analyses between the transcriptomes of stage-matched patagium, dorsal and shoulder skin from the sugar glider or plagiopatagium, and dorsal skin from Seba's short-tailed bat were performed using DeSeq2 v1.30.1 from BioConductor (https://bioconductor.org/) (*17*). For each analysis, the dataset was releveled such that the non-patagium comparison tissue (i.e., dorsal skin or shoulder) was set as the reference level so that patagium–up-regulated genes were expressed as positive $\log_2$ fold changes and patagium–down-regulated genes were negative. The DESeq2 function was called, resulting *P* values were conservatively adjusted for multiple testing using the Benjamini-Hochberg procedure (FDR < 0.01), and only genes showing at least a 1.5-fold change were considered differentially expressed. Gene Ontology analyses for genes up-regulated in the sugar glider lateral patagium or bat plagiopatagium were performed using the Gene Ontology Resource Web server (http://geneontology.org/) and the *M. musculus* biological process database. The term enrichment significance was determined by Fisher's exact test (FDR < 0.05). To explore potential links between observed sugar glider and bat patagium gene expression patterns and known mammalian developmental programs, we manually parsed our transcriptomic data to record the expression status of genes involved in the placode of the developing hair follicle and in the AER of the limbs. These programs were chosen as each is capable of driving phenotypes reminiscent of the patagium in different developmental contexts. The hair placode is characterized by a region of thickened epidermis and signals to underlying mesenchyme to control the formation of the dermal condensate, thus resembling the defining phenotypes of the patagium primordium. Similarly, the AER acts as a primary regulator of limb bud outgrowth, so we hypothesized that a similar signaling circuit could be at play during patagium outgrowth. These data are summarized in table S16. Briefly, we found limited evidence for redeployment of either program in the patagium. Many core AER FGFs were not expressed in the patagia of bats or sugar gliders, and while some hair placode genes were expressed, few showed differential expression compared to neighboring dorsal skin. Annotation liftover of *Dkk4* (a placode gene) to Seba's short-tailed bat was unsuccessful due to the low quality of the available genome assembly; thus, its expression status was not included for the bat.

Epidermal-dermal recombination explant cultures

Pouch young were collected at approximately P4. This stage was used as it represents the period before patagium outgrowth when dermal condensation becomes most defined and because enzymatic dissociation of live dermis and epidermis before this stage had a low rate of success. For each pouch young, patagium skin and dorsal skin were removed using fine dissecting scissors and ultrafine forceps. Each tissue was then floated in one well of a six-well plate containing 3 ml of Dulbecco's modified Eagle's medium (DMEM) (Corning, 10-017-CV) plus 0.3 g of dispase II (Sigma-Aldrich, D4693) with the epidermis facing upward and the dermis submerged in the media. Tissues were then incubated on a nutator rotating at 12 rpm for 2 hours at 37°C. At the 1-hour and 1.5-hour

marks, toothbrush bristles were used to gently tease apart epidermis and dermis to expose new surface area to the enzyme. After the dissociation was completed, tissues were transferred to wells of a fresh six-well plate with 3 ml of DMEM + 10% bovine calf serum (Cytiva HyClone, :SH3007203; hereafter BCS) and nutated at 12 rpm for 15 min at room temperature to wash away residual enzyme. A single Whatman Nucleopore Track-Etched Membrane (WHA110614) was placed in the lid of a sterile petri dish, and fine forceps were used to transfer a dermis (either patagium or dorsal control) into the dish. Forceps were used to slide the dermis onto flat paddle forceps (prewetted in DMEM + 10% BCS). The dermis was then gently slid onto the membrane. The wetted paddle forceps were then used to lift segments of dorsal epidermis from the surface of the wash media, and toothbrush bristles were used to spread it on top of the dermis. The whole membrane, recombined explant in place, was then transferred to a fresh six-well plate with 3 ml of DMEM + 10% BCS + 1% penicillin/streptomycin (Gibco, 15070-063). Two recombinations were performed, each with five replicates. Dorsal epidermis was recombined with patagium dermis to test the potential for patagium dermis to drive morphological changes in epidermis. As a negative control, dorsal epidermises were recombined with dorsal dermis. Explants were cultured for 96 hours, replacing media each day. Explants were then fixed while attached to the membrane filter in 4% PFA for approximately 4 hours before being processed (undergoing overnight incubations in 10% sucrose, 30% sucrose, 50:50 mix of 30% sucrose, and OCT) and embedded in OCT. Sectioning was performed as described above. Epidermal thickness was quantified using Fiji software by measuring the tissue stained with hematoxylin and eosin from the base of the epidermis to the top of the epidermis. We took a total of 10 measurements per tissue section, three tissue sections per sample, and five samples per treatment. Statistical significance was assessed using a general mixed effects model analysis of variance (ANOVA) test (fixed effect = treatment; random effect = individual per sample). Statistical significance was assigned to P values: $^{*}P < 0.05$, $^{**}P < 0.01$, $^{***}P < 0.001$, and $^{****}P < 0.0001$.

Bead implantation in dorsal skin explants

Bio-Rad Affi-Gel Blue Gel beads (100 μl; Bio-Rad, 1537301) were added to 1 ml of sterile PBS in a 2-ml low-bind tube (Eppendorf, 0030108450), vortexed briefly, and then centrifuged for 10 s in a microfuge. PBS was removed by pipetting, and the procedure was repeated two more times. Beads were then resuspended in a final volume of approximately 10 to 20 μl. Concentrated beads were then placed in a sterile petri dish, divided into two equal-sized droplets, and allowed to dry in a sterile hood for at least 2 hours. When beads were dry, they were resuspended in a protein solution. To test *Wnt5a* function, beads were soaked in 2 μl of a 50:50 mix of recombinant WNT5A (R&D Systems, 645-WN-010) at stock concentration of 1 μg/μl and PBS with BSA (50 μg/μl). For controls, beads were soaked in a BSA (25 μg/μl). Beads were incubated in their respective solutions at 4°C for 1.5 hours, during which time pouch young at approximately P4 were collected. Pouch young were euthanized 5 to 10 min before the end of bead incubation and placed under a dissecting scope. The bevel of a 31-gauge needle was then used to create several pockets into the dermis of the dorsal skin, into which beads were placed using sterile #55 forceps. After beads were placed, the dorsal skin was removed from the pouch young and placed onto Whatman filter membranes (Whatman, 131135012e) using forceps and toothbrush bristles and grown for 72 hours as explants floating on full media DMEM + 10% BCS + 1% penicillin/streptomycin. Explants were then fixed while attached to the membrane filter in 4% PFA for 3 hours before being processed for embedding and sectioning, as described above. Epidermal thickness was quantified using Fiji software by measuring the tissue stained with hematoxylin and eosin from the base of the epidermis to the top of the epidermis. We took a total of 10 measurements per tissue section, three tissue sections per sample, and five samples per treatment. The first two measurements were taken directly above the bead, with subsequent ones taken in opposite directions (four to the left of the bead and four to the right, equidistantly spaced). The statistical significance was assessed using a general mixed effects model ANOVA test (fixed effect = treatment; random effect = individual per sample). Statistical significance was assigned to P values: $^{*}P < 0.05$, $^{**}P < 0.01$, $^{***}P < 0.001$, and $^{****}P < 0.0001$.

Mouse experiments

Mouse strains

The following mouse strains were obtained from the Jackson laboratories: FVB/N-Tg(tetO-Wnt5a)17Rva/J (JAX, 022938) and B6.Cg *Gt(ROSA)26Sor*$^{tm1(rtTA*M2)Jae}$/J (JAX, 006965). Both males and females were used in the analysis. All mouse experiments were approved by the respective Institutional Animal Care and Use Committee at Princeton University and University of California, Irvine.

Induction of transgenes and tissue processing

For *Wnt5a* induction, P30 mice were placed on doxycycline (1 mg/ml) containing water ad libitum for 7 days (doxycycline water was replaced every other day). Tissues were fixed and processed for histology and IHC, as described for the sugar gliders and bats.

Phenotypic characterization

Wnt5a *transgenics*. Epidermal thickness was quantified using Fiji software by measuring the tissue stained with hematoxylin and eosin from the base of the epidermis to the top of the epidermis. Measurements were taken exclusively from interfollicular regions (10 measurements per dorsal skin section, three dorsal skins sections per sample, and four samples per treatment). Cell density was quantified on tissue sections by counting the number of DAPI^{+} cells per surface area (measurements were done on three dorsal skin sections per sample and four samples per treatment). Statistical significance was assessed using a general mixed effects model ANOVA test (fixed effect = treatment; random effect = individual per sample). Statistical significance was assigned to P values: $^{*}P < 0.05$, $^{**}P < 0.01$, $^{***}P < 0.001$, and $^{****}P < 0.0001$.

Ear pinna

Quantification of cell nuclei and epidermal thickness was done using the ImageJ software. Briefly, we counted all DAPI-stained cell nuclei in K14^{+} epidermis across different zones of the embryo head, including ear pinna. Epidermal thickness was measured using the measure tool to measure thickness of the K14^{+} layer across different zones of the embryo head (20 measurements per zone across the epidermis and three embryos). Statistical significance was assessed using a general mixed effects model ANOVA test (fixed effect = treatment; random effect = individual/sample). Statistical significance was assigned to P values: $^{*}P < 0.05$, $^{**}P < 0.01$, $^{***}P < 0.001$, and $^{****}P < 0.0001$.

Supplementary Materials

This PDF file includes:

Figs. S1 to S3
Tables S1 to S3, S15, and S16
Legends for tables S4 to S14
Legend for movie S1

Other Supplementary Material for this manuscript includes the following:

Tables S4 to S14
Movie S1

View/request a protocol for this paper from *Bio-protocol*.

REFERENCES AND NOTES

1. G. F. Gunnell, N. B. Simmons, *Evolutionary history of bats: fossils, molecules and morphology*. (Cambridge University Press, 2012).
2. R. W. Meredith, M. Westerman, M. S. Springer, A phylogeny of Diprotodontia (Marsupialia) based on sequences for five nuclear genes. *Mol. Phylogenet. Evol.* **51**, 554–571 (2009).
3. I. Casanovas-Vilar, J. Garcia-Porta, J. Fortuny, Ó. Sanisidro, J. Prieto, M. Querejeta, S. Llácer, J. M. Robles, F. Bernardini, D. M. Alba, Oldest skeleton of a fossil flying squirrel casts new light on the phylogeny of the group. *eLife* **7**, e39270 (2018).
4. J. Schmitz, M. Ohme, B. Suryobroto, H. Zischler, The colugo (*Cynocephalus variegatus*, Dermoptera): The primates' gliding sister? *Mol. Biol. Evol.* **19**, 2308–2312 (2002).
5. K. L. Bishop, Aerodynamic force generation, performance and control of body orientation during gliding in sugar gliders (*Petaurus breviceps*). *J. Exp. Biol.* **210**, 2593–2606 (2007).
6. R. W. Meredith, M. A. Mendoza, K. K. Roberts, M. Westerman, M. S. Springer, A phylogeny and timescale for the evolution of pseudocheiridae (Marsupialia: Diprotodontia) in Australia and New Guinea. *J. Mammal. Evol.* **17**, 75–99 (2010).
7. O. R. Bininda-Emonds, M. Cardillo, K. E. Jones, R. D. MacPhee, R. M. Beck, R. Grenyer, S. A. Price, R. A. Vos, J. L. Gittleman, A. Purvis, The delayed rise of present-day mammals. *Nature* **446**, 507–512 (2007).
8. K. Ferner, J. A. Schultz, U. Zeller, Comparative anatomy of neonates of the three major mammalian groups (monotremes, marsupials, placentals) and implications for the ancestral mammalian neonate morphotype. *J. Anat.* **231**, 798–822 (2017).
9. M. J. Smith, Petaurus breviceps. *Mammalian Species*, (1973), pp. 1–5.
10. N. I. Weisenfeld, V. Kumar, P. Shah, D. M. Church, D. B. Jaffe, Direct determination of diploid genome sequences. *Genome Res.* **27**, 757–767 (2017).
11. C. Holt, M. Yandell, MAKER2: An annotation pipeline and genome-database management tool for second-generation genome projects. *BMC Bioinformatics* **12**, 491 (2011).
12. R. N. Johnson, D. O'Meally, Z. Chen, G. J. Etherington, S. Y. W. Ho, W. J. Nash, C. E. Grueber, Y. Cheng, C. M. Whittington, S. Dennison, E. Peel, W. Haerty, R. J. O'Neill, D. Colgan, T. L. Russell, D. E. Alquezar-Planas, V. Attenbrow, J. G. Bragg, P. A. Brandies, A. Y.-Y. Chong, J. E. Deakin, F. Di Palma, Z. Duda, M. D. B. Eldridge, K. M. Ewart, C. J. Hogg, G. J. Frankham, A. Georges, A. K. Gillett, M. Govendir, A. D. Greenwood, T. Hayakawa, K. M. Helgen, M. Hobbs, C. E. Holleley, T. N. Heider, E. A. Jones, A. King, D. Madden, J. A. M. Graves, K. M. Morris, L. E. Neaves, H. R. Patel, A. Polkinghorne, M. B. Renfree, C. Robin, R. Salinas, K. Tsangaras, P. D. Waters, S. A. Waters, B. Wright, M. R. Wilkins, P. Timms, K. Belov, Adaptation and conservation insights from the koala genome. *Nat. Genet.* **50**, 1102–1111 (2018).
13. M. Stanke, O. Keller, I. Gunduz, A. Hayes, S. Waack, B. Morgenstern, AUGUSTUS: Ab initio prediction of alternative transcripts. *Nucleic Acids Res.* **34**, W435–W439 (2006).
14. N. A. O'Leary, M. W. Wright, J. R. Brister, S. Ciufo, D. Haddad, R. McVeigh, B. Rajput, B. Robbertse, B. Smith-White, D. Ako-Adjei, A. Astashyn, A. Badretdin, Y. Bao, O. Blinkova, V. Brover, V. Chetvernin, J. Choi, E. Cox, O. Ermolaeva, C. M. Farrell, T. Goldfarb, T. Gupta, D. Haft, E. Hatcher, W. Hlavina, V. S. Joardar, V. K. Kodali, W. Li, D. Maglott, P. Masterson, K. M. McGarvey, M. R. Murphy, K. O'Neill, S. Pujar, S. H. Rangwala, D. Rausch, L. D. Riddick, C. Schoch, A. Shkeda, S. S. Storz, H. Sun, F. Thibaud-Nissen, I. Tolstoy, R. E. Tully, A. R. Vatsan, C. Wallin, D. Webb, W. Wu, M. J. Landrum, A. Kimchi, T. Tatusova, M. DiCuccio, P. Kitts, T. D. Murphy, K. D. Pruitt, Reference sequence (RefSeq) database at NCBI: Current status, taxonomic expansion, and functional annotation. *Nucleic Acids Res* **44**, D733–D745 (2016).
15. P. Langfelder, S. Horvath, WGCNA: An R package for weighted correlation network analysis. *BMC Bioinformatics* **9**, 559 (2008).
16. H. Mi, X. Huang, A. Muruganujan, H. Tang, C. Mills, D. Kang, P. D. Thomas, PANTHER version 11: Expanded annotation data from Gene Ontology and Reactome pathways, and data analysis tool enhancements. *Nucleic Acids Res.* **45**, D183–D189 (2017).
17. M. I. Love, W. Huber, S. Anders, Moderated estimation of fold change and dispersion for RNA-seq data with DESeq2. *Genome Biol.* **15**, 550 (2014).
18. P. Maye, J. Zheng, L. Li, D. Wu, Multiple mechanisms for Wnt11-mediated repression of the canonical Wnt signaling pathway. *J. Biol. Chem.* **279**, 24659–24665 (2004).
19. X. Martineau, É. Abed, J. Martel-Pelletier, J.-P. Pelletier, D. Lajeunesse, Alteration of Wnt5a expression and of the non-canonical Wnt/PCP and Wnt/PKC-$Ca2^{+}$ pathways in human osteoarthritis osteoblasts. *PLOS ONE* **12**, e0180711 (2017).
20. C. Niehrs, Function and biological roles of the Dickkopf family of Wnt modulators. *Oncogene* **25**, 7469–7481 (2006).
21. R. A. Stewart, A.-B. Ramakrishnan, K. M. Cadigan, Diffusion and function of Wnt ligands. *PLOS Genet.* **15**, e1008154 (2019).
22. T. P. Yamaguchi, A. Bradley, A. P. McMahon, S. Jones, A Wnt5a pathway underlies outgrowth of multiple structures in the vertebrate embryo. *Development* **126**, 1211–1223 (1999).
23. J. L. Rinn, J. K. Wang, N. Allen, S. A. Brugmann, A. J. Mikels, H. Liu, T. W. Ridky, H. S. Stadler, R. Nusse, J. A. Helms, H. Y. Chang, A dermal HOX transcriptional program regulates site-specific epidermal fate. *Genes Dev.* **22**, 303–307 (2008).
24. J. E. Gudjonsson, A. Johnston, S. W. Stoll, M. B. Riblett, X. Xing, J. J. Kochkodan, J. Ding, R. P. Nair, A. Aphale, J. J. Voorhees, J. T. Elder, Evidence for altered wnt signaling in psoriatic skin. *J. Invest. Dermatol.* **130**, 1849–1859 (2010).
25. F. Tian, T. M. Mauro, Z. Li, The pathological role of Wnt5a in psoriasis and psoriatic arthritis. *J. Cell. Mol. Med.* **23**, 5876–5883 (2019).
26. Y. Yang, L. Topol, H. Lee, J. Wu, Wnt5a and Wnt5b exhibit distinct activities in coordinating chondrocyte proliferation and differentiation. *Development* **130**, 1003–1015 (2003).
27. S. Reddy, T. Andl, A. Bagasra, M. M. Lu, D. J. Epstein, E. E. Morrisey, S. E. Millar, Characterization of Wnt gene expression in developing and postnatal hair follicles and identification of Wnt5a as a target of Sonic hedgehog in hair follicle morphogenesis. *Mech. Dev.* **107**, 69–82 (2001).
28. R. van Amerongen, C. Fuerer, M. Mizutani, R. Nusse, Wnt5a can both activate and repress Wnt/β-catenin signaling during mouse embryonic development. *Dev. Biol.* **369**, 101–114 (2012).
29. K. Hochedlinger, Y. Yamada, C. Beard, R. Jaenisch, Ectopic expression of Oct-4 blocks progenitor-cell differentiation and causes dysplasia in epithelial tissues. *Cell* **121**, 465–477 (2005).
30. R. F. O'Shaughnessy, A. M. Christiano, Inherited disorders of the skin in human and mouse: From development to differentiation. *Int. J. Dev. Biol.* **48**, 171–179 (2004).
31. M. Tokita, T. Abe, K. Suzuki, The developmental basis of bat wing muscle. *Nat. Commun.* **3**, 1302 (2012).
32. S. M. Jackson, Glide angle in the genus Petaurus and a review of gliding in mammals. *Mamm. Rev.* **30**, 9–30 (2000).
33. R. Zeller, J. López-Ríos, A. Zuniga, Vertebrate limb bud development: Moving towards integrative analysis of organogenesis. *Nat. Rev. Genet.* **10**, 845–858 (2009).
34. Y. Gañan, D. Macias, R. D. Basco, R. Merino, J. M. Hurle, Morphological diversity of the avian foot is related with the pattern of msx gene expression in the developing autopod. *Dev. Biol.* **196**, 33–41 (1998).
35. I. R. Cordeiro, R. Yu, M. Tanaka, Regulation of the limb shape during the development of the Chinese softshell turtles. *Evol. Dev.* **22**, 451–462 (2020).
36. S. D. Weatherbee, R. R. Behringer, J. J. t. Rasweiler, L. A. Niswander, Interdigital webbing retention in bat wings illustrates genetic changes underlying amniote limb diversification. *Proc. Natl. Acad. Sci. U.S.A.* **103**, 15103–15107 (2006).
37. C. Minguillon, J. Del Buono, M. P. Logan, Tbx5 and Tbx4 are not sufficient to determine limb-specific morphologies but have common roles in initiating limb outgrowth. *Dev. Cell* **8**, 75–84 (2005).
38. S. Tümpel, J. J. Sanz-Ezquerro, A. Isaac, M. C. Eblaghie, J. Dobson, C. Tickle, Regulation of Tbx3 expression by anteroposterior signalling in vertebrate limb development. *Dev. Biol.* **250**, 251–262 (2002).
39. M. Osterwalder, D. Speziale, M. Shoukry, R. Mohan, R. Ivanek, M. Kohler, C. Beisel, X. Wen, S. J. Scales, V. M. Christoffels, A. Visel, J. Lopez-Rios, R. Zeller, HAND2 targets define a network of transcriptional regulators that compartmentalize the early limb bud mesenchyme. *Dev. Cell* **31**, 345–357 (2014).
40. L. Panman, A. Galli, N. Lagarde, O. Michos, G. Soete, A. Zuniga, R. Zeller, Differential regulation of gene expression in the digit forming area of the mouse limb bud by SHH and gremlin 1/FGF-mediated epithelial-mesenchymal signalling. *Development* **133**, 3419–3428 (2006).
41. L. Zhou, J. Liu, P. Olson, K. Zhang, J. Wynne, L. Xie, Tbx5 and Osr1 interact to regulate posterior second heart field cell cycle progression for cardiac septation. *J. Mol. Cell. Cardiol.* **85**, 1–12 (2015).
42. P. Vallecillo-García, M. Orgeur, S. vom Hofe-Schneider, J. Stumm, V. Kappert, D. M. Ibrahim, S. T. Börno, S. Hayashi, F. Relaix, K. Hildebrandt, G. Sengle, M. Koch, B. Timmermann,

G. Marazzi, D. A. Sassoon, D. Duprez, S. Stricker, Odd skipped-related 1 identifies a population of embryonic fibro-adipogenic progenitors regulating myogenesis during limb development. *Nat. Commun.* **8**, 1218 (2017).
43. G. R. Martin, The roles of FGFs in the early development of vertebrate limbs. *Genes Dev.* **12**, 1571–1586 (1998).
44. H. S. Bruce, N. H. Patel, Knockout of crustacean leg patterning genes suggests that insect wings and body walls evolved from ancient leg segments. *Nat. Ecol. Evol.* **4**, 1703–1712 (2020).
45. C. M. Nelson, On buckling morphogenesis. *J. Biomech. Eng.* **138**, 021005 (2016).
46. T. Tallinen, J. Y. Chung, J. S. Biggins, L. Mahadevan, Gyrification from constrained cortical expansion. *Proc. Natl. Acad. Sci. U.S.A.* **111**, 12667–12672 (2014).
47. S. A. Montandon, A. Fofonjka, M. C. Milinkovitch, Elastic instability during branchial ectoderm development causes folding of the Chlamydosaurus erectile frill. *eLife* **8**, e44455 (2019).
48. S. B. Carroll, Evo-devo and an expanding evolutionary synthesis: A genetic theory of morphological evolution. *Cell* **134**, 25–36 (2008).
49. M. Malekian, S. J. B. Cooper, J. A. Norman, L. Christidis, S. M. Carthew, Molecular systematics and evolutionary origins of the genus Petaurus (Marsupialia: Petauridae) in Australia and New Guinea. *Mol. Phylogenet. Evol.* **54**, 122–135 (2010).
50. T. Cremona, A. M. Baker, S. J. B. Cooper, R. Montague-Drake, A. M. Stobo-Wilson, S. M. Carthew, Integrative taxonomic investigation of Petaurus breviceps (Marsupialia: Petauridae) reveals three distinct species. *Zool. J. Linn. Soc.* **191**, 503–527 (2020).
51. C. D. Campbell, J. Pecon-Slattery, R. Pollak, L. Joseph, C. E. Holleley, The origin of exotic pet sugar gliders (Petaurus breviceps) kept in the United States of America. *PeerJ* **7**, e6180 (2019).
52. S. Jackson, C. Groves, *Taxonomy of Australian Mammals*. (2015).
53. M. Seppey, M. Manni, E. M. Zdobnov, BUSCO: Assessing genome assembly and annotation completeness. *Methods Mol. Biol.* **1962**, 227–245 (2019).
54. C. Feigin, S. Frankenberg, A. Pask, A chromosome-scale hybrid genome assembly of the extinct Tasmanian tiger (Thylacinus cynocephalus). *Genome Biol. Evol.* **14**, evac048 (2022).
55. B. J. Haas, A. Papanicolaou, M. Yassour, M. Grabherr, P. D. Blood, J. Bowden, M. B. Couger, D. Eccles, B. Li, M. Lieber, M. D. MacManes, M. Ott, J. Orvis, N. Pochet, F. Strozzi, N. Weeks, R. Westerman, T. William, C. N. Dewey, R. Henschel, R. D. LeDuc, N. Friedman, A. Regev, De novo transcript sequence reconstruction from RNA-seq using the Trinity platform for reference generation and analysis. *Nat. Protoc.* **8**, 1494–1512 (2013).
56. I. Korf, Gene finding in novel genomes. *BMC Bioinformatics* **5**, 59 (2004).
57. N. Renier, Z. Wu, D. J. Simon, J. Yang, P. Ariel, M. Tessier-Lavigne, iDISCO: A simple, rapid method to immunolabel large tissue samples for volume imaging. *Cell* **159**, 896–910 (2014).
58. T. J. Pisano, Z. M. Dhanerawala, M. Kislin, D. Bakshinskaya, E. A. Engel, E. J. Hansen, A. T. Hoag, J. Lee, N. L. de Oude, K. U. Venkataraju, J. L. Verpeut, F. E. Hoebeek, B. D. Richardson, H. J. Boele, S. S. Wang, Homologous organization of cerebellar pathways to sensory, motor, and associative forebrain. *Cell Rep.* **36**, 109721 (2021).
59. Y. Isogai, S. Si, L. Pont-Lezica, T. Tan, V. Kapoor, V. N. Murthy, C. Dulac, Molecular organization of vomeronasal chemoreception. *Nature* **478**, 241–245 (2011).
60. J. J. T. Rasweiler, C. J. Cretekos, R. R. Behringer, Whole-mount immunohistochemistry of short-tailed fruit bat (*Carollia perspicillata*). *Cold Spring Harb. Protoc.* **2009**, pdb.prot5167 (2009).
61. S. Picelli, O. R. Faridani, Å. K. Björklund, G. Winberg, S. Sagasser, R. Sandberg, Full-length RNA-seq from single cells using Smart-seq2. *Nat. Protoc.* **9**, 171–181 (2014).
62. A. M. Bolger, M. Lohse, B. Usadel, Trimmomatic: A flexible trimmer for Illumina sequence data. *Bioinformatics* **30**, 2114–2120 (2014).
63. A. Dobin, C. A. Davis, F. Schlesinger, J. Drenkow, C. Zaleski, S. Jha, P. Batut, M. Chaisson, T. R. Gingeras, STAR: Ultrafast universal RNA-seq aligner. *Bioinformatics* **29**, 15–21 (2013).
64. A. Shumate, S. L. Salzberg, Liftoff: Accurate mapping of gene annotations. *Bioinformatics* **37**, 1639–1643 (2021).
65. O. Dudchenko, S. S. Batra, A. D. Omer, S. K. Nyquist, M. Hoeger, N. C. Durand, M. S. Shamim, I. Machol, E. S. Lander, A. P. Aiden, E. L. Aiden, De novo assembly of the Aedes aegypti genome using Hi-C yields chromosome-length scaffolds. *Science* **356**, 92–95 (2017).

Acknowledgments: We thank Princeton LAR (K. Gerhart, G. Barnett, and J. McGuire) for help with sugar glider husbandry, the LSI Genomics Core (J. M. Miller and J. Arley Volmar) for help with library preparation and sequencing, T. Pisano for help with tissue clearing and light-sheet imaging, F. Rogers for help with statistics, J. Scheibe for the access to initial sugar glider samples, and E. Ireland for proofreading. **Funding:** This project was supported by an NIH grant to R.M. (R35GM133758). C.Y.F. was supported by an NIH fellowship (F32 GM139240-01). M.V.P. is supported by LEO Foundation grants LF-AW-RAM-19-400008 and LF-OC-20-000611, W.M. Keck Foundation grant WMKF-5634988, NSF grant DMS1951144, and NIH grants U01-AR073159, R01-AR079150, and P30-AR075047. **Author contributions:** R.M. and C.Y.F. conceived the study and designed experiments. J.C., R.R.B., and J.J.R. provided bat tissues. B.O. provided initial sugar glider tissues. C.Y.F., A.A., S.A.M., J.A.M., B.O., and R.M. performed phenotypic characterization and histological analyses of sugar glider and bat tissues. R.M. generated the light-sheet movie. W.W. designed the sequencing strategy for sugar glider and bat transcriptomic samples and for the sugar glider genome. C.Y.F. performed all computational analyses, including assembly and assessment of the sugar glider genome, generation of gene annotations for sugar glider and bat, design of sugar glider in situ hybridization probes, as well as the design and execution of all transcriptomic analyses in both the sugar glider and bat. C.Y.F. conducted tissue recombination and bead implantation experiments in sugar glider explants. S.A.M., R.v.A, R.R., M.V.P., and R.M. conducted mouse experiments and phenotypic characterizations. R.M., A.A., and C.Y.F. generated data visualizations. R.M. supervised the project and provided administration. R.M. and C.Y.F. curated the data generated in the study. C.Y.F. and R.M. wrote the manuscript with input from all other authors. **Competing interests:** The authors declare that they have no competing interests. **Data and materials availability:** The sugar glider genome assembly and corresponding genome sequencing reads are submitted under NCBI BIoProject PRJNA849992. RNA-seq reads for the sugar glider and Seba's short-tailed bat are submitted under NCBI BioProjects PRJNA927154 and PRJNA859189, respectively. Genome annotations for the sugar glider and Sebat's short-tailed bat as well as the code used for differential expression and WGCNA analyses are available in the following FigShare repository: https://figshare.com/s/d6c585fbae0c1f22e8df. All data needed to evaluate the conclusions in the paper are present in the paper and/or the Supplementary Materials.

Submitted 5 September 2022
Accepted 21 February 2023
Published 24 March 2023
10.1126/sciadv.ade7511